



UNIVERSITY OF LEEDS

This is a repository copy of *The Atmospheric Coupling and Dynamics Across the Mesopause (ACaDAME) mission*.

White Rose Research Online URL for this paper:
<http://eprints.whiterose.ac.uk/152724/>

Version: Accepted Version

Article:

Janches, D, Yu, AW, Krainak, MA et al. (11 more authors) (2019) The Atmospheric Coupling and Dynamics Across the Mesopause (ACaDAME) mission. *Advances in Space Research*, 64 (10). pp. 1915-1925. ISSN 0273-1177

<https://doi.org/10.1016/j.asr.2019.07.012>

Published by Elsevier Ltd on behalf of COSPAR. This manuscript version is made available under the CC-BY-NC-ND 4.0 license
<http://creativecommons.org/licenses/by-nc-nd/4.0/>.

Reuse

This article is distributed under the terms of the Creative Commons Attribution-NonCommercial-NoDerivs (CC BY-NC-ND) licence. This licence only allows you to download this work and share it with others as long as you credit the authors, but you can't change the article in any way or use it commercially. More information and the full terms of the licence here: <https://creativecommons.org/licenses/>

Takedown

If you consider content in White Rose Research Online to be in breach of UK law, please notify us by emailing eprints@whiterose.ac.uk including the URL of the record and the reason for the withdrawal request.



eprints@whiterose.ac.uk
<https://eprints.whiterose.ac.uk/>

The Atmospheric Coupling and Dynamics Across the Mesopause (ACaDAME) Mission

D. Janches^a, A.W. Yu^b, M.A. Krainak^b, C. Gardner^c, B. Kaifler^d, S. Etemad^e,
D.C. Fritts^f, S.D. Eckermann^g, R.L. Collins^h, E.C.M. Dawkins^{a,i}, R.S.
Lieberman^a, D.R. Marsh^j, G. Liu^{a,i}, W. Jarvis^k

^a*ITM Laboratory, Heliophysics Science Division, GSFC/NASA, Greenbelt, MD 20771, USA*

^b*Laser & Electro-Optics Branch, GSFC/NASA, Greenbelt, MD 20771, USA*

^c*Department of Electrical and Computer Engineering, University of Illinois, Urbana, IL 61801, USA*

^d*Institute for Physics of the Atmosphere, German Space Center (DLR), Oberpfaffenhofen, Germany*

^e*Project Formulation & Development Office, GSFC/NASA, Greenbelt, MD 20771, USA*

^f*Global Atmospheric Technologies and Science (GATS), Inc., Boulder, CO, USA*

^g*Space Science Division, U.S. Naval Research Laboratory, Washington, DC 20375, USA*

^h*Geophysical Institute, University of Alaska, Fairbanks, Fairbanks, AK, USA*

ⁱ*Dept. of Physics and Astronomy, Catholic University of America, Washington, DC, USA*

^j*National Center for Atmospheric Research, Boulder, CO, USA*

^k*New Opportunities Office, GSFC/NASA, Greenbelt, MD 20771, USA*

Abstract

The Atmospheric Coupling and Dynamics Across the Mesopause (ACaDAME) is a mission designed to uniquely address critical questions involving multi-scale wave dynamics at key space weather (SWx) “gateway altitudes” of the mesosphere and lower thermosphere (MLT) at ~ 70 –150 km. ACaDAME observes with a nadir-pointing resonant lidar that utilizes the fluorescence of atomic Na present in the MLT. By tuning a laser to the Na absorption wavelength (589 nm), ACaDAME would perform very high resolution measurements of temperature and Na densities across the mesopause during both day and night. In this manner, Na is used as tracer for observing and characterizing MLT waves generated by tropospheric weather that represent the dominant terrestrial source of energy and momentum affecting space weather and transport of mesospheric species.

Keywords: lidar, MLT dynamics, gravity waves, planetary waves tides,

1. Introduction

Due to an ongoing lack of observational knowledge of key dynamical wave drivers, our ability to model and predict the Earth’s upper atmosphere above ~ 100 km altitude lags far behind the atmosphere below ~ 60 km. Like lower atmospheric weather prediction, the ability to predict the “space weather” (SWx) of the thermosphere-ionosphere (TI) system from ~ 80 -500 km altitude is essential, and now urgently needed, to support and protect our interconnected technological society, as has been recognized through the recent creation of a National Space Weather Strategy and Action Plan (Jonas and McCarron, 2016). Intense radiation and energetic particles from the Sun are absorbed in the thermosphere, providing not only a protective barrier sustaining life on the surface, but also ions and electrons that form the ionosphere. For many years it was widely believed that solar and geomagnetic variations in extraterrestrial energy inputs to the TI dominated its SWx. In recent years, however, that conventional wisdom has been upended by new research showing that atmospheric waves propagating into the TI from the lower atmosphere provide the dominant energy and momentum inputs relevant to its SWx. Such waves are now thought to account for up to 70% of the total energy injected into the TI (Liu, 2016) and for at least 50% of the ionosphere’s observed space-time “weather-related” variability (Forbes et al., 2000; Rishbeth and Mendillo, 2001). Even under highly disturbed geomagnetic conditions, atmospheric waves from lower atmospheric sources remain critical drivers and regulators of the TI’s global response and variability (Pedatella, 2016; Pedatella and Liu, 2018).

Solar energy absorbed in the lower atmosphere leads to the generation of upward-propagating solar tides and Rossby waves, which have planetary scale, and of smaller-scale gravity waves (GWs) with horizontal wavelengths of 20-500 km. Some of these planetary waves (PWs), tides and GWs propagate deep into the TI to drive its large-scale flow, structure, and variability (Figure 1). Thus atmospheric dynamics driven by solar inputs at lower altitudes represent “reprocessed” solar energy inputs into the TI that are competitive with direct

solar inputs from above. These PWs and tides are now believed to drive intense TI responses to stratospheric sudden warmings and trigger formation of sporadic ion layers closely related to contemporaneous sporadic sodium (Na) layers.

Small-scale GWs are the primary energy and momentum inputs from below, whose propagation into the TI is modified to a great degree by variations in PWs and tides. Key GW-driven TI SWx phenomena, such as traveling ionospheric disturbances and plasma bubbles, can affect electromagnetic wave propagation between ground sites and satellites, and hence disrupt communication, navigation and geolocation technologies essential to many aspects of modern life. Because these GWs and PWs are generated primarily by lower atmospheric weather events, lower atmospheric weather has strong influences on the SWx of the TI. Understanding the SWx of the TI is important not just for general scientific research and discovery, but also critical for applications such as spacecraft launch and reentry, suborbital experimental vehicles, and orbit prediction

2. The ACaDAMe Mission of Opportunity

ACaDAMe is a Mission of Opportunity proposal to deploy a high-power Na resonance lidar on the International Space Station (ISS). In doing so, the ACaDAMe mission would be the first to quantify critical multi-scale wave dynamics at the key SWx “gateway altitudes” of the mesosphere and lower thermosphere (MLT) at $\sim 70\text{--}150$ km. These wave processes drive the weather and climate of the entire MLT and, in the process, control and define the morphology of the surviving wave spectrum that propagates deep into the TI to drive SWx from below. Through near-global targeted measurement of the critical gateway altitudes from $\sim 70\text{--}150$ km, ACaDAMe would quantify the complex nonlinear multi-scale wave interactions that drive the entire transport circulation, chemical composition, climate and weather of the MLT across scales (Fritts and Alexander, 2003; Garcia and Solomon, 1985; Garcia et al., 2014), and, in the process, determine the surviving PW and GW spectrum that propagates to higher altitudes to drive TI SWx from below (Liu, 2016; Pedatella et al., 2014).

ACaDAME observations would answer fundamental questions about wave-driven dynamics and species transport in the MLT, such as momentum and energy deposition and associated diffusive transport, while also clarifying how these multi-scale wave dynamics organize the morphology of a surviving wave spectrum that propagates deep into the TI to drive SWx from below. In particular, ACaDAME measurements would address the following overarching Science Goals (SGs):

- Quantify for the first time the near-global distribution of GWs, including their amplitudes, scales, and energy and momentum fluxes (MFs), that impact the MLT and are major terrestrial drivers of SWx.
- Quantify for the first time the near-global interactions of MLT GWs with tides and PWs that impact these larger-scale motions and determine the spectrum of GWs entering and impacting the TI.
- Characterize the impact of wave-induced transport on the main mesospheric Na layer, the chemical-dynamical drivers of sporadic Na layers and thermospheric Na plumes.

ACaDAME would measure MLT temperatures (T) and Na densities (ρ_{Na}) with high vertical and horizontal resolution, night and day, primarily at altitudes $z \sim 75\text{--}105$ km. These measurements would capture not only the characteristics of waves that propagate through the MLT and drive the TI from below, but also the characteristics of GWs that deposit the dominant momentum and energy in the MLT and determine its weather and climate across scales. ACaDAME would also provide considerable insight on the dominant role that these waves play in transporting key species like atomic oxygen, nitric oxide and the meteoric metals to lower altitudes where they have important impacts on chemical and radiative balance, stratospheric cloud formation, ozone depletion and possibly the global CO₂ cycle. The unique combination of T and ρ_{Na} measurements from ACaDAME would quantify eddy transport and chemical-dynamical coupling by GWs. ACaDAME would also measure thermospheric Na plumes that extend above the mesopause, allowing additional determinations of neutral temperature

and wave activity up to ~ 170 km altitude (Chu et al., 2011).

3. Instrument Description

ACaDAME employs a nadir-pointing lidar (see Figure 2) with a single 589 nm transmitter with a field-of-view (FOV) of $150 \mu\text{rad}$, co-boresighted with the receiver aperture. The receiver aperture provides a $200 \mu\text{rad}$ FOV. The transceiver assembly accommodates the laser transmitter and telescope receiver, as well as the thermal control system. As depicted in Figure 3, the Payload Interface Unit (PIU) attaches to the Japanese Experiment Module-External Facility (JEM-EF) on the ISS, and within the JEM-EF.

ACaDAME’s functional block diagram as shown in Figure 3, consists of a laser transmitter, an optical receiver, an electronics box and thermal control mounted on an optical bench. ACaDAME uses laser pulses tuned to three frequencies within the 589-nm-wavelength Na D₂ absorption-line, to resonantly excite fluorescence of Na atoms in the MLT. The backscattered fluorescence signals are collected by a telescope, passed through an optical filter assembly to reject background noise, and captured by eight photon-counting detectors. The photon counts are range-resolved via time-of-flight measurements. Altitude profiles of T , ρ_{Na} , and Doppler shift are derived from the photon count profiles measured at the three different laser frequencies.

The lidar requirements to meet the engineering (cost, schedule, ISS platform) and science objectives described earlier are listed in Table 1.

3.1. Mesospheric T and ρ_{Na} Measurements

Vertical profiles of T and ρ_{Na} in the MLT, as well as the Doppler shift associated with off-nadir pointing, are obtained by probing the thermally broadened absorption cross-section of meteoric Na (Figure 4) at three different frequencies, specifically 1) the D_{2a} peak (ν_{pk}), 2) the minimum between the D_{2a} and D_{2b} peaks (ν_{min}), and 3) at the frequency (ν_{int}) between ν_{pk} and ν_{min} . This value of ν_{min} varies with T and so it is chosen for 190 K, the mean mesopause value at

mid-latitudes. The detected photon counts are proportional to the product of ρ_{Na} and the absorption cross-section, which depends on T and the Doppler shift associated with off-nadir pointing. T , ρ_{Na} , and Doppler shift are derived from the signal counts using well-known techniques for solving sets of nonlinear equations. The approach is equivalent to solving the lidar equation for the values of T , ρ_{Na} , and Doppler shift for which the theoretically calculated signal count equals the measured count, simultaneously at all three laser frequencies (Gardner and Vargas, 2014). The calculation of associated errors in T and ρ_{Na} is well established (Papen et al., 1995; Chu and Papen, 2005; Gardner and Vargas, 2014). In particular, the Root Mean Square (RMS) T and ρ_{Na} errors for the nadir-pointing three-frequency ACaDAME configuration are

$$\Delta T_{RMS} = \begin{cases} \frac{387K}{\sqrt{SNR_{pk}}} & \text{at night} \\ \frac{695K}{\sqrt{SNR_{pk}}} & \text{at day} \end{cases} \quad (1)$$

$$\frac{(\Delta\rho_{Na})_{RMS}}{\rho_{Na}} = \begin{cases} \frac{127\%}{\sqrt{SNR_{pk}}} & \text{at night} \\ \frac{150\%}{\sqrt{SNR_{pk}}} & \text{at day} \end{cases} \quad (2)$$

$$SNR_{pk} = \frac{N_{pk}^2}{N_{pk} + N_n + N_D} = \frac{(0.164\rho_{Na}/cm^{-3})^2(\Delta z/km)(\Delta s/km)}{(0.164\rho_{Na}/cm^{-3} + 261(R_B + R_D)/MHz)} \quad (3)$$

where N_B is the background count per resolution cell, N_D is the corresponding dark count, N_{pk} is the signal count when the laser is tuned to ν_{pk} , $R_D \sim 0.02$ MHz is the detector dark count rate and R_B is the background count rate. R_B depends on the Earth's albedo, solar zenith angle and the ACaDAME optical bandwidth and is ~ 12 MHz for an albedo of 0.3, solar zenith angle of 45° and optical full-width half-maximum (FWHM) bandwidth of 30 GHz. Note that the background noise for ACaDAME was estimated by assuming that the Earth is a Lambertian reflector of the incident sunlight and by taking into account the strong solar Fraunhofer line centered at the Na D₂ wavelength. These noise contributions must be measured and subtracted from the backscattered signal and the results normalized by the Rayleigh backscattered signal from the

lower stratosphere. ACaDAME measures the noise level between 190 and 250 km altitude and the Rayleigh signal between 30 and 42 km (Figure 5). The low Rayleigh signal can only be measured at night, which is acceptable, as it is used to calibrate the overall throughput of the transmitter and receiver, which varies slowly with time. The pulse energies are also measured and used to normalize the backscattered signals.

ACaDAME’s performance on ISS is comparable to the highest-performance ground-based systems currently in use. For example, the Na Doppler lidar at Tromsø, Norway employs the same solid-state laser technology (4.15 W at 589 nm) as that proposed for ACaDAME (Kawahara et al., 2017). This lidar has a power-aperture product of about 0.40 Wm², compared to ACaDAME’s 1.22 Wm². When the effects of the increased target distance for ACaDAME on ISS (factor of 3) and the 2-way atmospheric attenuation and detector quantum efficiency (QE) of the Tromsølidar (~ 0.33) are considered, the signal-to-noise ratios (SNRs) of the two systems are comparable. Additionally, ACaDAME’s background noise is ~ 4 times smaller than that of a space-based aerosol/cloud lidar with a similar aperture, FOV, and etalon bandwidth operating at 532 nm, where there is no Fraunhofer line. Thus, ACaDAME’s laser technology and measurement performance (SNR) are comparable to the best ground-based systems currently in operation (Kawahara et al., 2017) but would provide near-global high resolution observations. Additionally, its daytime noise performance would be better (~ 6 dB smaller) than similar space-based aerosol/cloud lidars like the Cloud-Aerosol Transport System (CATS) (Storm et al., 2016).

Equations 1 and 2 provide a theoretical estimate of the measurement errors which are summarized in Table 2, where Δz and Δs represent the vertical and along-the-track resolutions and λ_z and λ_s are the GWs vertical and horizontal wavelengths. We also assessed ACaDAME’s performance with an end-to-end simulation, taking into account all instrument parameters and atmospheric phenomena of interest, and simulating the detected signals. ACaDAME acquires data at high resolution that can then be additionally averaged along track or in altitude to yield lower errors for studies of the waves specific to the individual

wave regimes. Figure 6 shows the expected errors in T retrieval (ΔT_{Mean}), averaged from 86 to 98 km altitude, where ρ_{Na} is largest, as a function of vertical and horizontal integration. These errors are computed using a typical annual-mean ρ_{Na} profile and are plotted in Figure 6. The dotted areas in Figure 6 represent the combination of ground post-processing resolutions which would satisfy science requirements. Thus the errors would be lower than required to achieve the SGs and ACaDAME would exceed both the error and resolution requirements of the science mission. These end-to-end error estimates are consistent with the error in Eq. 1 and 2 averaged over 86-99 km and can be approximated by

$$\Delta T_{Mean} = \frac{16.9\text{K}(\text{km}^{-1})}{\sqrt{\Delta z(\text{km})\Delta s(\text{km})}} \quad (4)$$

3.2. Detection of Gravity Waves (GWs)

To study GW dynamics in the MLT, we characterize the perturbations in T and ρ_{Na} induced by individual GWs and by a spectrum of GWs. Individual GW amplitudes typically vary from several K to over 30 K in the MLT (Cao and Liu, 2016) while the temperature variance induced by the full spectrum of GWs can vary between 30 and 150 K² (Gardner and Liu, 2007). Decades of MLT observations have shown that ρ_{Na} and T are usually dominated by one or two prominent waves, which can be readily characterized using spectral techniques such as the S-Transform (Stockwell et al., 1996). In these cases the measurement precision is usually limited by photon and background noise. The GW polarization and dispersion relations can be used to relate the temperature amplitude T' of a GW to its MF per unit mass, as follows

$$\frac{2N_0T_0}{g}\sqrt{MF} = 0.882K\sqrt{MF(m^2/s^2)} \leq T'(K) \quad (5)$$

where N_0 is the **background buoyancy frequency**, T_0 is the background temperature and MF is the **momentum flux**. Both N_0 and T_0 would be measured by ACaDAME. To confirm that ACaDAME can characterize the scientifically important waves, we assume that the GW amplitude is determined

by fitting sinusoids to T at each altitude along the orbit track and then average the results. We focus on the altitude range where SNR is largest, and assume the sinusoidal fit is made over 3 along-track oscillations of the wave. To achieve the scientific goals, requires the measurement precision of T' to be less than 20% at night, in which case it would also be possible to determine the other wave parameters (e.g. λ_z , λ_s and MF) with adequate precision. Thus, using the lower bound on T' given by the **left hand side** (LHS) of Eq. 5, we find that

$$\Delta T_{Mean}(\Delta z, \Delta s) \leq 0.938K \sqrt{\frac{\lambda_h(km)MF(m^2/s^2)}{\Delta z(km)\Delta s(km)}} \quad (6)$$

The **right hand side** (RHS) of Eq. 6 represents the scientific requirement for GW observations (Figure 6 and Table 2).

An extensive database of MLT GWs observed over Maui, HI and Cerro Pachón (Cao and Liu, 2016), showed that the most probable GWs had $\lambda_h \sim 30$ km, $\lambda_z \sim 25$ km and intrinsic periods ~ 7 min. Approximately 67% of the GWs had MF magnitudes exceeding $\sim 20 \text{ m}^2\text{s}^{-2}$. Thus, to characterize 67% of GWs at night, ACaDAME must resolve MFs as low as $20 \text{ m}^2\text{s}^{-2}$ and $\lambda_h \sim$ as short as 20 km. According to Eq. 6, to accomplish this the average measurement precision (between 86 and 98 km at $\Delta z=2$ km and $\Delta s=3$ km) must be 7.7 K or smaller. At night, according to Eq. 4, ACaDAME would achieve 6.9 K so that even for the smallest scale ($\lambda_s=20$ km) **and** smallest amplitude GW (MF= $20 \text{ m}^2\text{s}^{-2}$ and $T'=3.9$ K), its amplitude would be determined with a precision better than 20% (less than 0.8 K). The science requirements and performance capabilities for the full range of phenomena studied by ACaDAME are summarized in Table 2.

In addition to the theoretical estimates given by Eqs. 5 and Eq. 6, we also estimated the atmospheric response to GWs via a simulation in which we added prescribed wave-induced perturbations to a background T_0 profile. The resulting T field was then probed using a model of the ACaDAME measurement. The T profile was retrieved from the output of this model, and binned in the same way as ACaDAME level 0 data. The retrieved T were high-pass filtered

to isolate GWs. Finally, we determined T' , λ_z , and λ_s using harmonic fits and compared to the original GW parameter (Figure 7). A series of these simulations show that ACaDAME can characterize GWs with amplitudes as low as 3.5 K at altitudes where ρ_{Na} is highest if there is a coherent wave pattern with at least three along-track oscillations.

3.3. Doppler Shifts and ACaDAME Performance

ACaDAME would point approximately perpendicular to the ISS velocity vector and would experience a small relativistic transverse Doppler effect (160 MHz), given the ~ 7 km/s ISS orbit speed, which would be considered in the T retrieval. The ISS pitches, yaws and rolls around the velocity vector, changing the pointing direction of the laser. Changes in pitch would tilt the laser off-nadir and induce a Doppler shift, detuning the Na-absorption from the source wavelength. During space shuttle docking, the ISS changed attitude by up to ± 122 mrad ($\pm 7^\circ$) (Treder, 1999; Budzien et al., 2011), but this no longer occurs.

Figure 4b shows the Doppler Na absorption cross-section in the ISS reference frame for different off-nadir angles. Detuning is significant for large angles (~ 800 MHz at 3.5°). However, the chosen frequency separation guarantees that ACaDAME measurements are highly sensitive to thermal broadening of the Na absorption, and thus T , over a large range of off-nadir angles. Figure 8 illustrates simulated ACaDAME performance as a function of off-nadir angle. Between -1° and $+4^\circ$, temperature errors vary by less than 30%. Our initial calculations show that ACaDAME can tolerate changes in the ISS pitch angle over a range of about 4-5 degrees and still achieve a measurement precision sufficient to address the SGs. The Na fluorescence received by ACaDAME's receiver telescope would also be Doppler-shifted but the etalon filter bandwidth is many times wider, and thus the transmission is essentially constant over this small range. The intensity-dependent Doppler effect is also very small at orbital velocities and contributes less than a 0.01% change in intensity when the velocity vector and source direction are parallel.

3.4. Na Vapor Physics

Saturation, radiation pressure, and optical pumping can all limit fluorescence return and require corrections for the T and ρ_{Na} calculations. For saturation, as the laser pulse energy increases, the fraction of Na atoms in excited states increases to a limiting value. There are three approaches to reduce saturation: 1) increase the laser bandwidth, 2) increase the beam width, or 3) increase the pulse length. Considerable research exists (Holzlöhner et al., 2010; Rampy et al., 2015; Hellemeier et al., 2017) on the engineering of laser parameters for optimizing the Na fluorescence for laser guide stars. For ACaDAMe, the goal is to limit saturation effects to minimize T and ρ_{Na} errors. Initial calculations show saturation effects are minimal.

4. ACaDAMe Design

4.1. ACaDAMe Laser Transmitter

The ACaDAMe design includes a single-frequency tunable laser transmitter. The transmitter consists of a Laser Optics Module (LOM) and a Laser Electronics Module (LEM). To produce the required 589 nm laser light, the transmitter mixes the outputs of two diode-pumped Nd:YAG lasers – one at 1064 nm and one at 1319 nm, since $1/589 = 1/1064 + 1/1319$. The sum frequency generation (SFG) is performed in a nonlinear optical crystal of Lithium triborate (LiB₃O₅), denoted LBO. The Ice, Cloud, and land Elevation / Geoscience Laser Altimeter System (ICESat/GLAS) (Afzal et al., 2007), CATS (Chuang et al., 2013; Storm et al., 2016) and ICESat-2/ Advanced Topographic Laser Altimeter System (ATLAS) (Konoplev et al., 2016) spaceflight laser transmitters also used an LBO crystal to produce 532 nm light. NASA-GSFC solid-state Q-switched Nd:YAG lasers were designed, built and tested in-house for the GLAS (Afzal et al., 2007), Mercury Laser Altimeter (MLA) (Krebs et al., 2005), Lunar Orbiter Laser Altimeter (LOLA) (Yu et al., 2008) and Global Ecosystem Dynamics Investigation (GEDI) (Coyle et al., 2015) missions. Each ICESat/GLAS space-

flight Nd:YAG laser transmitter produced 4.5W of total optical power at 1064 nm and 532 nm (Afzal et al., 2007).

Numerous 589 nm lasers using SFG have been constructed, including the fielded Na-lidar SFG diode-pumped laser with very similar architecture and requirements to ACaDAME, operating in Tromsø (Kawahara et al., 2017). This TRL-5 lidar has a laser output power of ~ 4 W at one of 3 tunable wavelength and a laser pulse width of 35 ns with linewidth < 200 MHz, similar to ACaDAME’s specifications (Table 1) (Kawahara et al., 2017; Krainak et al., 2018). ACaDAME’s SFG laser transmitter wavelength outputs scheme, mixing specific wavelengths output from the 1064 nm and 1319 nm lasers, by alternatively operates each of the acousto-optic frequency shifters (AOFS) for individual seed lasers as shown in Figure 9 and schematically in Figure 10. ACaDAME’s SFG Q-switched laser operates at 300 Hz to ensure no range ambiguity. The SFG Q-switched laser wavelength is rapidly tuned between successive laser pulses (Figure 9) so the laser alternates between three closely-spaced wavelengths (Table 1). This is accomplished via injection-seeding and locking. At the receiver, this allows measurement of the Na-resonant lidar signal returns in time bins, such that returns from each wavelength are separated and sorted in the time domain.

4.2. Laser Optics Module (LOM)

The LOM is a robust platform that houses all of the laser optical and optomechanical components (Figure 11). To rapidly tune three fixed laser wavelengths at the Na-resonant D_2 line, each of the Nd:YAG lasers were injection seeded with electronically-switchable seed lasers near 1064 nm and 1319 nm. The wavelength stability of the 589 nm laser pulses is achieved by locking the wavelength of the injection seeder to the D_{2a} absorption line (Figure 10). The D_{2a} absorption line is detected by the modulation transfer spectroscopy (MTS) technique. The signal is fed back to one of the seed lasers to ensure the summed frequency (wavelength) is always at 589.15900 nm (D_{2a} or λ_{pk}). Wavelength switching to λ_{min} at 589.15790 nm is achieved by frequency-shifting the 1064

nm seed laser using AOFS₁, which is designed to provide a shift of frequency of 951 MHz (see table in Figures 9 and 10), and an optical switch. Wavelength switching to the intermediate wavelength, λ_{int} at 589.15846 nm, is achieved by frequency-shifting the 1319 nm seed laser using AOFS₂, which is designed to provide a frequency shift of 467 MHz, and an optical switch. Through the operating conditions of the AOFS₁ and AOFS₂ in the ON and OFF state for the each of the seed lasers as shown in Figure 9, the wavelengths of the seed lasers would then be used to injection seed the corresponding Nd:YAG cavities as shown in Figure 11. The cavities are locked to the incoming laser frequency by the Pound-Drever-Hall method (Drever et al., 1983). Figure 12 shows experimental absolute frequency-locking performance demonstrated by our prototype system (Numata et al., 2011; Riris et al., 2017; Abshire et al., 2018). It has achieved <5 MHz drift over >24 hours, satisfying the <40 MHz requirement for <2K temperature measurement accuracy.

4.3. Laser Electronics Module (LEM)

The LEM serves as the electrical interface between the laser and the instrument power and data systems. Its primary function is to deliver regulated 200 μ s, 100 A pulses to the laser diodes. The LEM is composed of four major subassemblies, each with a dedicated printed circuit card: 1) the internal converter; 2) the boost converter; 3) the control electronics, and; 4) the thermal control board. These four cards, the energy storage capacitor bank, the field-effect-transistor (FET) heat sink structure, and associated internal harnessing are packaged within the electronics cavity of the laser assembly chassis.

4.4. Transmission Optics

The ACaDAME transmission optics consist of a Beam Expander telescope and a Boresight Alignment Mechanism (BAM). The BAM, which is a set of Risley prisms mounted in an opto-mechanical rotation mechanism, ensures the instrument boresight alignment by applying post-launch pointing corrections to the transmitted beam. The boresight alignment requirement is $\pm 5 \mu$ rad.

4.5. Receiver Telescope, Aft Optics and Detector System Module

ACaDAME would use a Ritchey-Chretien beryllium telescope as a receiver telescope. A 0.6 m beryllium primary mirror collects the resonant-Na fluorescence and background. A secondary mirror directs the beam towards the aft-optics (Figure 13).

The light from the receiver telescope output is collimated by two lenses and directed through an Optical Filter Assembly (OFA; Figure 13). The OFA is critical to reduce the background sunlight reflected by the Earth and scattered by the atmosphere, enabling daytime measurements. The OFA consists of a 0.2 nm FWHM optical bandpass filter and a 0.028 nm FWHM temperature-tuned etalon interference filter in series (Troupaki et al., 2015; Zaun et al., 2004). The OFA also provides a means to monitor the etalon-to-laser wavelength tracking. Three additional lenses focus the filtered light onto a fiber optic, which relays it to the detector system electronics module (DSEM).

ACaDAME uses eight solid-state single-photon-counting modules (SPCMs) to detect the Na-resonant fluorescence signal. The SPCMs use a low-noise Si avalanche photodiode operated in Geiger mode. The dynamic range of the received signal and background light require eight SPCMs to prevent saturation during daytime measurements. The optical signal output from the filter assembly is equally divided into eight SPCMs by a set of non-polarizing beam-splitters. A compound lens focuses the light onto the SPCMs. The DSEM Data Capture Card (DCC): 1) ingests the SPCM data up to a maximum total photon count rate of $160 \text{ Mcps} = 20 \text{ Mcps/SPCM} \times 8 \text{ SPCMs}$, 2) implements Multichannel Scaler (MCS) time binning, and 3) implements the SPCM Gate Control. This system may be optimized to achieve more uniform error responses (Figure 5) or, if needed, to increase the range of pitch angles that ACaDAME can tolerate.

5. Conclusions

The proposed ACaDAME Mission of Opportunity would focus on the full spectrum of atmospheric waves, with scales from local to global, that travel

from the troposphere upwards towards geospace. On their way these waves will interact with each other and the background atmosphere. Some will be absorbed, driving the winds and temperatures in the MLT and determining the distribution of energetically important chemicals and metals, while others will continue upward to interact and modify the TI, and have SWx impacts. The ISS provides an ideal combination of altitude, geographic, and local time (LT) coverage to accomplish the ACaDAME science goals, through near-global measurements. Most ACaDAME subsystems leverage technology validated during the successful Clouds and Aerosol Transport System (CATS) mission. A high Technology Readiness Level (TRL) design, ample ISS-provided resources within margin, and technological innovation leveraging NASA GSFC expertise in space-based laser measurements, offer a low-cost solution to providing the necessary measurements to achieve this high-impact ACaDAME science.

Acknowledgments

This work has been supported by the NASA HTIDeS program and NASA/GSFC IRAD and B&P program. SDE acknowledges support for this work from the Chief of Naval Research.

References

- Abshire, J.B., Ramanathan, A.K., Riris, H., Allan, G.R., Sun, X., Hasselbrack, W.E., Mao, J., Wu, S., Chen, J., Numata, K., Kawa, S.R., Yang, M.Y.M., DiGangi, J., 2018. Airborne measurements of CO₂ column concentrations made with a pulsed IPDA lidar using a multiple-wavelength-locked laser and HgCdTe APD detector. *Atmospheric Measurement Techniques* 11, 2001–2025. doi:10.5194/amt-11-2001-2018.
- Afzal, R.S., Yu, A.W., Dallas, J.L., Melak, A., Lukemire, A.T., Ramos-Izquierdo, L., Mamakos, W., 2007. The Geoscience Laser Altimeter System (GLAS) Laser Transmitter. *IEEE Journal of Selected Topics in Quantum Electronics* 13, 511–536. doi:10.1109/JSTQE.2007.896051.

- Budzien, S.A., Stephan, A.W., Bishop, R.L., Christensen, A.B., Hecht, J.H., Minschwaner, K.R., 2011. The RAIDS experiment on the ISS: on-orbit performance, in: *Solar Physics and Space Weather Instrumentation IV*.
- Cao, B., Liu, A.Z., 2016. Intermittency of gravity wave momentum flux in the mesopause region observed with an all-sky airglow imager. *Journal of Geophysical Research (Atmospheres)* 121, 650–663. doi:10.1002/2015JD023802.
- Chu, X., Papen, G., 2005. Resonance Fluorescence Lidar for Measurements of the Middle and Upper Atmosphere. pp. 179–432.
- Chu, X., Yu, Z., Gardner, C.S., Chen, C., Fong, W., 2011. Lidar observations of neutral Fe layers and fast gravity waves in the thermosphere (110–155 km) at McMurdo (77.8°S, 166.7°E), Antarctica. *Geophys. Res. Lett.* 38, 23807. doi:10.1029/2011GL050016.
- Chuang, T., Burns, P., Walters, E.B., Wysocki, T., Deely, T., Losse, A., Le, K., Drumheller, B., Schum, T., Hart, M., Puffenburger, K., Ziegler, B., Hovis, F., 2013. Space-based, multi-wavelength solid-state lasers for NASA’s Cloud Aerosol Transport System for International Space Station (CATS-ISS), in: *Solid State Lasers XXII: Technology and Devices*, p. 85990N. doi:10.1117/12.2005545.
- Coyle, D.B., Stysley, P.R., Poullos, D., Clarke, G.B., Kay, R.B., 2015. Laser transmitter development for NASA’s Global Ecosystem Dynamics Investigation (GEDI) lidar, in: *Lidar Remote Sensing for Environmental Monitoring XV*, p. 961208. doi:10.1117/12.2191569.
- Drever, R.W.P., Hall, J.L., Kowalski, F.V., Hough, J., Ford, G.M., Munley, A.J., Ward, H., 1983. Laser phase and frequency stabilization using an optical resonator. *Applied Physics B: Lasers and Optics* 31, 97–105. doi:10.1007/BF00702605.

- Forbes, J.M., Palo, S.E., Zhang, X., 2000. Variability of the ionosphere. *Journal of Atmospheric and Solar-Terrestrial Physics* 62, 685–693. doi:10.1016/S1364-6826(00)00029-8.
- Fritts, D.C., Alexander, M.J., 2003. Gravity wave dynamics and effects in the middle atmosphere. *Reviews of Geophysics* 41, 1003. doi:10.1029/2001RG000106.
- Garcia, R.R., López-Puertas, M., Funke, B., Marsh, D.R., Kinnison, D.E., Smith, A.K., González-Galindo, F., 2014. On the distribution of CO₂ and CO in the mesosphere and lower thermosphere. *Journal of Geophysical Research (Atmospheres)* 119, 5700–5718. doi:10.1002/2013JD021208.
- Garcia, R.R., Solomon, S., 1985. The effect of breaking gravity waves on the dynamics and chemical composition of the mesosphere and lower thermosphere. *J. Geophys. Res.* 20, 3850–3868.
- Gardner, C., Vargas, F., 2014. Optimizing three-frequency Na, Fe, and He lidars for measurements of wind, temperature, and species density and the vertical fluxes of heat and constituents. *Appl. Opt.* 53, 4100. doi:10.1364/AO.53.004100.
- Gardner, C.S., Liu, A.Z., 2007. Seasonal variations of the vertical fluxes of heat and horizontal momentum in the mesopause region at Starfire Optical Range, New Mexico. *Journal of Geophysical Research (Atmospheres)* 112, 9113. doi:10.1029/2005JD006179.
- Hellemeier, J.A., Hickson, P., Labadie, L., 2017. Modeling the response of mesospheric sodium to pulsed-laser excitation. *Journal of the Optical Society of America A* 34, 1376. doi:10.1364/JOSAA.34.001376.
- Holzlohner, R., Rochester, S.M., Bonaccini Calia, D., Budker, D., Higbie, J.M., Hackenberg, W., 2010. Optimization of cw sodium laser guide star efficiency. *A&A* 510, A20. doi:10.1051/0004-6361/200913108, arXiv:0908.1527.

- Jonas, S., McCarron, E.D., 2016. White House Releases National Space Weather Strategy and Action Plan. *Space Weather* 14, 54–55. doi:10.1002/2015SW001357.
- Kawahara, T.D., Nozawa, S., Saito, N., Kawabata, T., Tsuda, T.T., Wada, S., 2017. Sodium temperature/wind lidar based on laser-diode-pumped Nd:YAG lasers deployed at Tromsø, Norway (69.6°N, 192°E). *Optics Express* 25, A491. doi:10.1364/OE.25.00A491.
- Konoplev, O.A., Chiragh, F.L., Vasilyev, A.A., Edwards, R., Stephen, M.A., Troupaki, E., Yu, A.W., Krainak, M.A., Sawruk, N., Hovis, F., Culpepper, C.F., Strickler, K., 2016. Three-year aging of prototype flight laser at 10 kHz and 1 ns pulses with external frequency doubler for ICESat-2 mission, in: *Laser Technology for Defense and Security XII*, p. 98340A. doi:10.1117/12.2225985.
- Krainak, M.A., Yu, A.W., Li, S.X., Bai, Y., Numata, K., Chen, J.R., Fahey, M.E., Micalizzi, F., Konoplev, O.A., Janches, D., Gardner, C.S., Allan, G.R., 2018. Progress on laser technology for proposed space-based sodium lidar, in: *Solid State Lasers XXVII: Technology and Devices*, p. 105111E. doi:10.1117/12.2290471.
- Krebs, D.J., Novo-Gradac, A.M., Li, S.X., Lindauer, S.J., Afzal, R.S., Yu, A.W., 2005. Compact, passively Q-switched Nd:YAG laser for the MESSENGER mission to Mercury. *Applied Opt.* 44, 1715–1718. doi:10.1364/AO.44.001715.
- Liu, H.L., 2016. Variability and predictability of the space environment as related to lower atmosphere forcing. *Space Weather* 14, 634–658. doi:10.1002/2016SW001450.
- Numata, K., Chen, J.R., Wu, S.T., Abshire, J.B., Krainak, M.A., 2011. Frequency stabilization of distributed-feedback laser diodes at 1572 nm for lidar measurements of atmospheric carbon dioxide. *Applied Opt.* 50, 1047. doi:10.1364/AO.50.001047.

- Papen, G.C., Pfenninger, W.M., Simonich, D.M., 1995. Sensitivity analysis of Na narrowband wind-temperature lidar systems. *App. Opt.* 34, 480. doi:10.1364/AO.34.000480.
- Pedatella, N.M., 2016. Impact of the lower atmosphere on the ionosphere response to a geomagnetic superstorm. *Geophys. Res. Lett.* 43, 9383–9389. doi:10.1002/2016GL070592.
- Pedatella, N.M., Fuller-Rowell, T., Wang, H., Jin, H., Miyoshi, Y., Fujiwara, H., Shinagawa, H., Liu, H.L., Sassi, F., Schmidt, H., Matthias, V., Goncharenko, L., 2014. The neutral dynamics during the 2009 sudden stratosphere warming simulated by different whole atmosphere models. *Journal of Geophysical Research (Space Physics)* 119, 1306–1324. doi:10.1002/2013JA019421.
- Pedatella, N.M., Liu, H.L., 2018. The Influence of Internal Atmospheric Variability on the Ionosphere Response to a Geomagnetic Storm. *Geophys. Res. Lett.* 45, 4578–4585. doi:10.1029/2018GL077867.
- Rampy, R., Gavel, D., Rochester, S.M., Holzlohner, R., 2015. Toward optimization of pulsed sodium laser guide stars. *Journal of the Optical Society of America B Optical Physics* 32, 2425. doi:10.1364/JOSAB.32.002425, arXiv:1510.04982.
- Riris, H., Numata, K., Wu, S., Gonzalez, B., Rodriguez, M., Scott, S., Kawa, S., Mao, J., 2017. Methane optical density measurements with an integrated path differential absorption lidar from an airborne platform. *Journal of Applied Remote Sensing* 11, 034001. doi:10.1117/1.JRS.11.034001.
- Rishbeth, H., Mendillo, M., 2001. Patterns of F2-layer variability. *Journal of Atmospheric and Solar-Terrestrial Physics* 63, 1661–1680. doi:10.1016/S1364-6826(01)00036-0.
- Stockwell, R.G., Masinha, L., Lowe, R.P., 1996. Localization of the complex spectrum: The *S* transform. *IEEE TRANSACTIONS ON SIGNAL PROCESSING* 44, 998–1001.

- Storm, M., Stevenson, G., Hovis, F., Gavert, W., Dang, X., Darab, A., Chuang, T., Burns, P., 2016. Lidar and Laser Technology for NASA'S Cloud-Aerosol Transport System (CATS) Payload on The International Space Station (JEM-EF), in: European Physical Journal Web of Conferences, p. 04002. doi:10.1051/epjconf/201611904002.
- Treder, A.J., 1999. Space station GN&C overview for payloads, in: El-Genk, M.S. (Ed.), Space Technology and Applications, International Forum – 1999, pp. 49–57. doi:10.1063/1.57616.
- Troupaki, E., Denny, Z.H., Wu, S., Bradshaw, H.N., Smith, K.A., Hulst, J.A., Ramos-Izquierdo, L.A., Cook, W.B., 2015. Space qualification of the optical filter assemblies for the ICESat-2/ATLAS instrument, in: Components and Packaging for Laser Systems, p. 93460H. doi:10.1117/12.2077839.
- Yu, A.W., Novo-Gradac, A.M., Shaw, G.B., Unger, G., Ramos-Izquierdo, L.A., Lukemire, A., 2008. The lunar orbiter laser altimeter (LOLA) laser transmitter, in: Solid State Lasers XVII: Technology and Devices, p. 68710D. doi:10.1117/12.779825.
- Zaun, N.H., Weimer, C., Sidorin, Y., Lunt, D., 2004. Solid-etalon for the CALIPSO lidar receiver, in: Barnes, W.L., Butler, J.J. (Eds.), Earth Observing Systems IX, pp. 141–145. doi:10.1117/12.559883.

Table 1: Set of lidar parameters and the necessary performance requirements in order to meet the all objectives, including science, technical, programmatic, as well as safety.

Lidar Parameter	Requirements
Laser Wavelength (interleaved pulses)	589.1579 nm, 589.1583 nm, 589.1590 nm
Pulse Energy, Full power beam energy	15 mJ, 4.5 W single beam
Laser pulse width and repetition rate	~30 ns at 300Hz
Laser Power (Electrical Total)	123W
Beam divergence angle	150 μ rad FWHM
Single Receiver telescope	60 cm diameter
Optical Receiver FOV	200 μ rad FW
Receiver optics transmission	>75%
Optical band-pass filter width	30 GHz FWHM
Detector Quantum Efficiency	>55% QE at 589 nm
Detector Array Maximum Photon-Count-Rate	160 Mcps (8x20 Mcps)
Detector Dark count rate	~20 kHz
Timing electronics timing resolution	100 Ms/s /channel binning
Laser Linewidth	85 MHz RMS

Table 2: Science requirements and ACaDAME performance.

Phenomenon/ Feature	Δz	Δs	Science Requirements	ACaDAME Precision	Margin
Fast GWs ($20 \text{ km} \leq \lambda_z \leq 20 \text{ km}$ & $\leq \lambda_h$)	5 km	3 km	$\Delta T_{Mean} \leq 5 \text{ K}$	4 K at night	25%
Medium GWs ($10 \text{ km} \leq \lambda_z \leq 30 \text{ km}$ & $50 \text{ km} \leq \lambda_h$)	2 km	3 km	$\Delta T_{Mean} \leq 12 \text{ K}$	7 K at night	71%
Slow GWs ($4 \text{ km} \leq \lambda_z \leq 16 \text{ km}$ & $100 \text{ km} \leq \lambda_h$)	1 km	5 km	$\Delta T_{Mean} \leq 19 \text{ K}$	8 K at night	140 %
Tides and PWs	5 km	500 km	$\Delta T_{Mean} \leq 2 \text{ K}$	0.3 K at night	667%
	5 km	500 km	$\Delta T_{Mean} \leq 2 \text{ K}$	1.5 K at day	33%
Global T Map	3 km	500 km	$\Delta T_{Mean} \leq 2.5 \text{ K}$	0.4 K at night	525%
	3 km	500 km	$\Delta T_{Mean} \leq 2.5 \text{ K}$	2.0 K at day	25%
Global ρ_{Na} Map	3 km	500 km	$(\Delta \rho_{Na})_{Mean} \leq$ 1%	0.2% at night	400%
	3 km	500 km	$(\Delta \rho_{Na})_{Mean} \leq$ 1%	0.5% at day	100%
Sporadic Na	1 km	5 km	$(\Delta \rho_{Na})_{Mean} \leq$ 5%	2.48% at night	102%
	2 km	20 km	$(\Delta \rho_{Na})_{Mean} \leq$ 5%	2.78% at day	80%
Thermospheric Na ($2 \text{ cm}^{-3} \leq \rho_{Na}$)	10 km	200 km	$\frac{\Delta \rho_{Na}}{\Delta N_a} \leq 30\%$	$\leq 28.0\%$ at night	23%

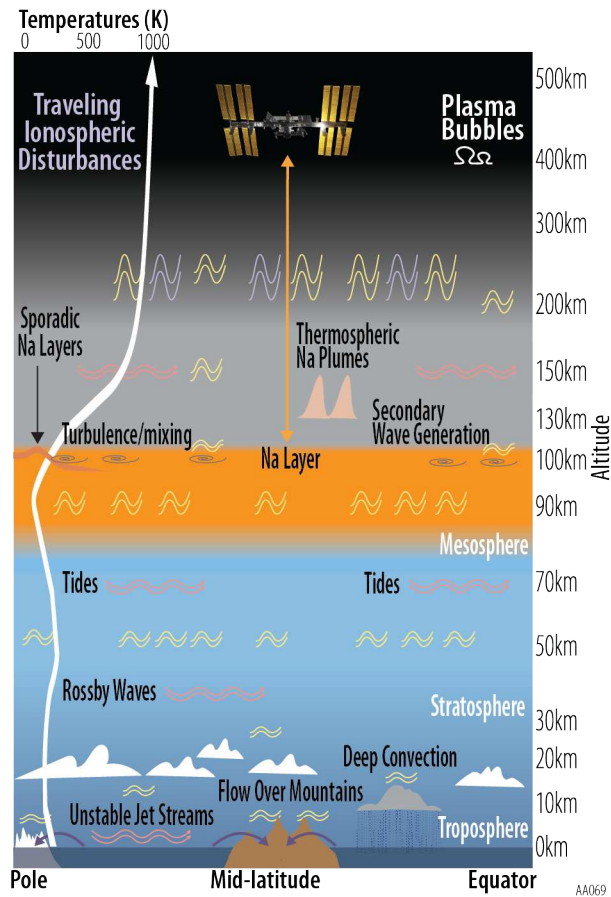
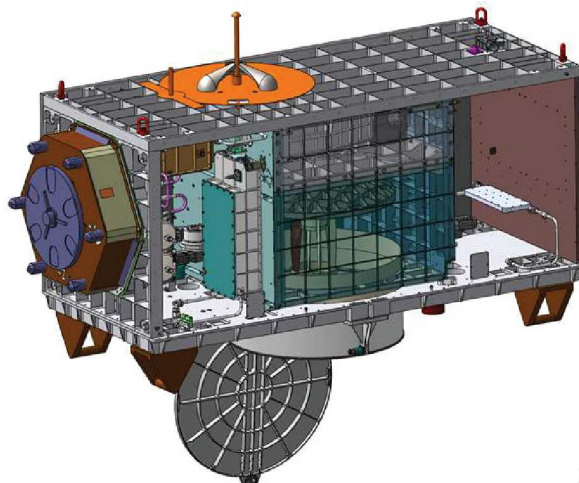
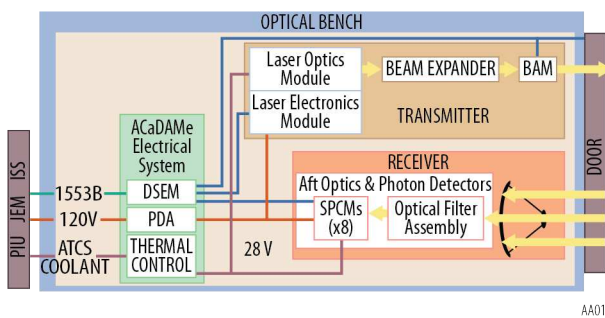


Figure 1: GW coupling processes in the atmosphere-ionosphere system versus altitude and latitude. Note the Na layer (orange), originates from the daily ablation of incoming meteoroids, where ACADEME would measure small- and large- scale waves and quantify their global momentum transport and deposition, multi-scale interactions, forcing of the MLT, and penetration to higher altitudes for the first time.



AA052

Figure 2: ACaDAME Flight System Concept.



AA014

Figure 3: ACaDAME lidar block diagram.

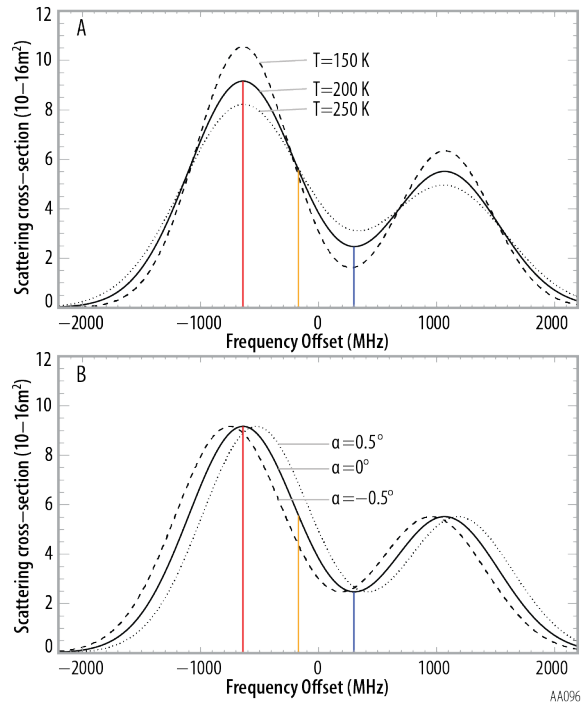


Figure 4: The Na D2 resonance line is a thermally broadened doublet composed of six hyperfine lines of atomic Na centered at 589.159 nm: (a) Earth's Na absorption cross-section as observed by ACaDAME on ISS at three different temperatures, and (b) at three different nadir angles. The chosen frequencies guarantee high sensitivity to thermal broadening of the Na line for a wide range of expected nadir pointing angles.

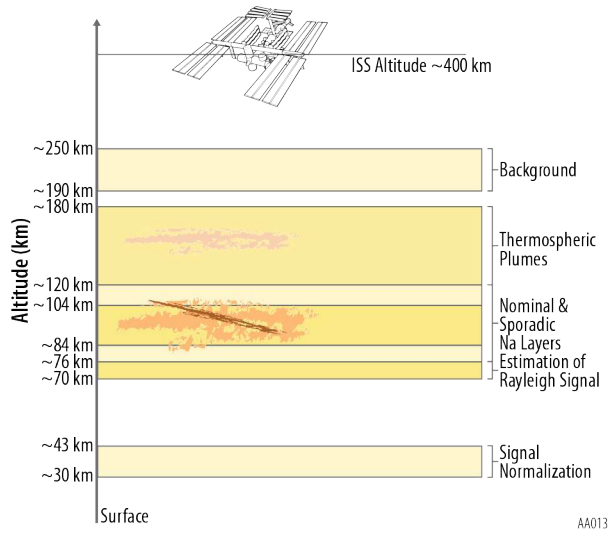


Figure 5: Regions of the atmosphere, and purpose. where ACADEME would perform measurements.

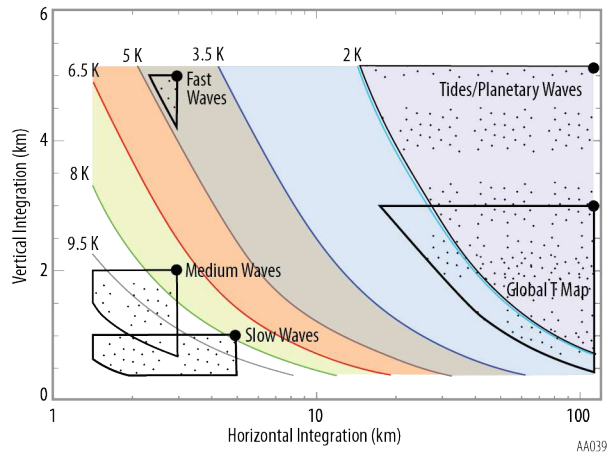


Figure 6: Expected nighttime T errors as function of vertical and horizontal integration and data sets required for proposed studies.

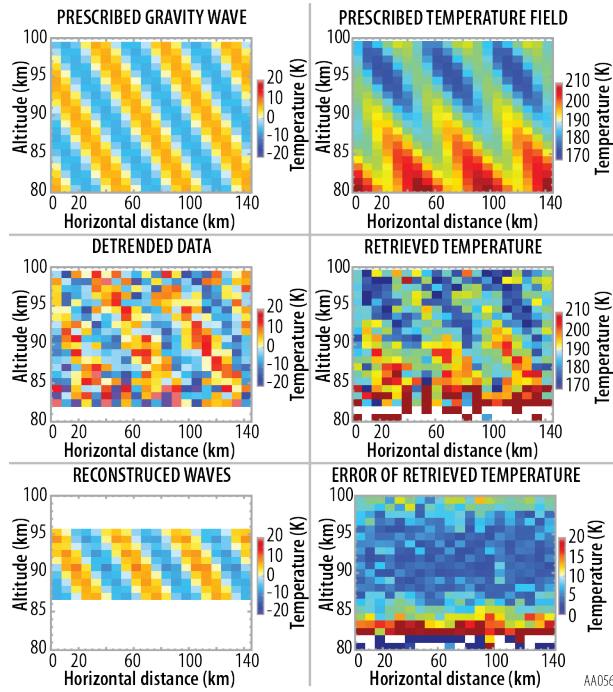


Figure 7: Example of an end-to-end simulation demonstrating ACaDAME's ability to detect GWs. The retrieval yielded GW parameters $T=7.3$ K, $\lambda_s = 48.6$ km and $\lambda_z = 14.3$ km, which are very similar to the prescribed values $T = 7.0$ K, $\lambda_s = 50.0$ km, and $\lambda_z = 15.0$ km.

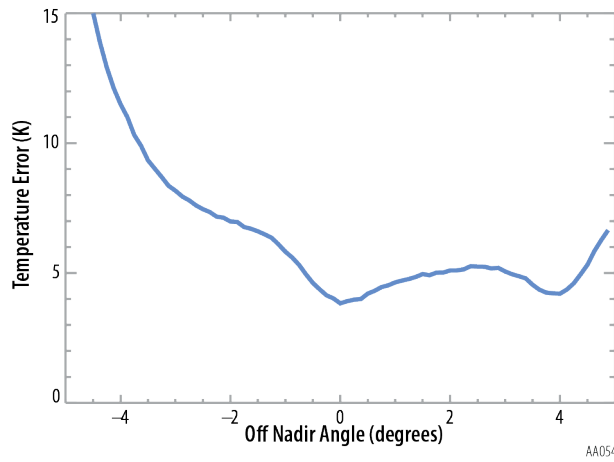


Figure 8: Simulated ACaDAME performance ($\Delta z=2.4$ km, $\Delta s=7.5$ km) as function of off nadir-angle. The temperature error between 86 and 98 km altitude is approximately flat between -1° and $+4^\circ$.

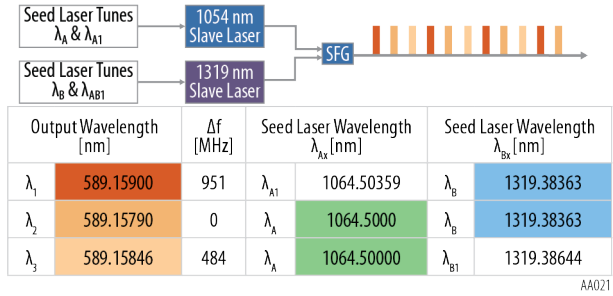


Figure 9: ACaDAME Laser Transmitter – frequency division multiplexing of the three transmitted wavelengths.

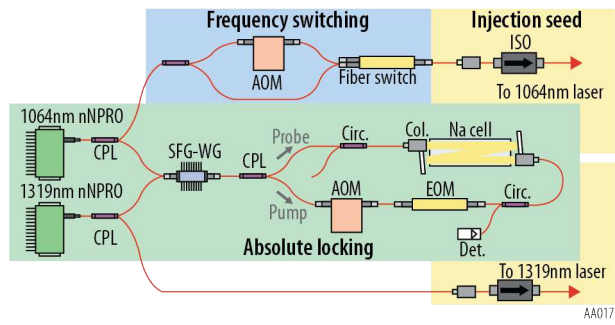


Figure 10: ACaDAME laser injection-seeding and wavelength locking system.

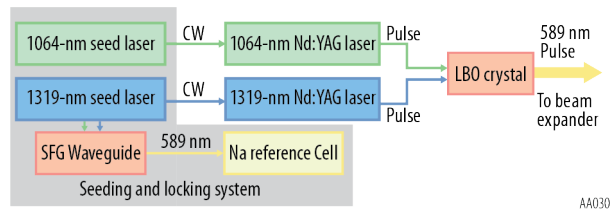


Figure 11: ACaDAME Laser Optics Module block diagram.

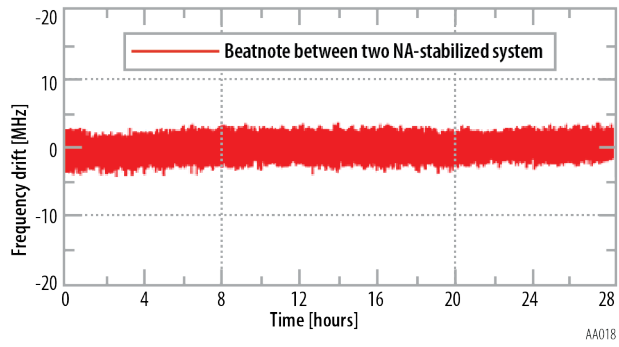


Figure 12: Experimental absolute frequency locking performance. The demonstrated <5 MHz drift surpasses the ACaDAMe requirement (<40 MHz).

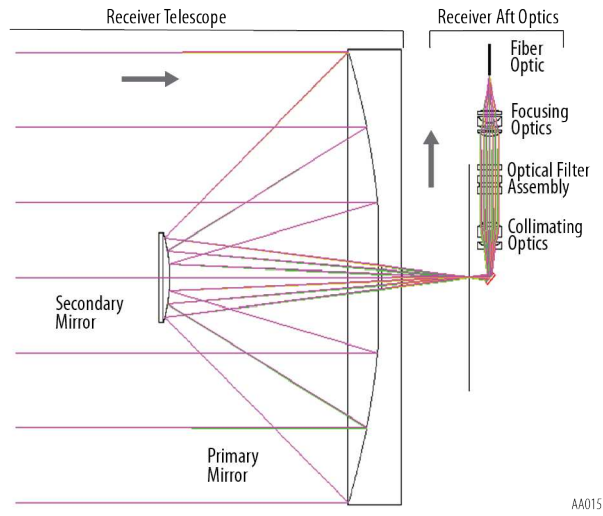


Figure 13: ACaDAMe Receiver Aft Optics design.